Semiclassical description of protonium formation in antiproton collisions with molecular hydrogen

W. A. Beck*
MicroConnex Corporation, Snoqualmie, Washington 98065, USA

L. Wilets
Department of Physics, University of Washington, Seattle, Washington 98195, USA

M. A. Alberg
Department of Physics, Seattle University, Seattle, Washington 98122, USA
and Department of Physics, University of Washington, Seattle, Washington 98195, USA
(Received 3 May 2006; revised manuscript received 1 October 2006; published 9 November 2006)

In a departure from our previous work modeling antiproton capture on helium, with its relatively straightforward, fixed center target, extending the semiclassical approach to molecular hydrogen, a multicenter target with target masses identical to the projectile, requires that we reconsider the fundamental nature of our model, in particular the momentum-dependent Heisenberg core used to stabilize electrons in the ground state. Here we discuss the main features of our Kirschbaum-Wilets model of molecular hydrogen as it is calibrated against proton collision data, and then used to study antiproton collisions. Details of the collision process are presented, including the energy and angular momentum states of incident antiprotons that result in formation of $p\bar{p}$, and the resulting distribution of protonium atomic states.

DOI: 10.1103/PhysRevA.74.052706 PACS number(s): 34.10.+x, 36.10.−k, 31.15.Gy, 34.50.Bw

I. INTRODUCTION

Protonium, the antiproton-proton atomic structure, is the simplest neutral baryonic system, quite analogous to leptonic positronium. The x-ray spectrum of protonium, utilizing lasers, provides an opportunity to study antiproton properties and the interaction of antiprotons with protons to high precision. Newly available low-energy antiproton beams (of the order of 10 eV) colliding with atomic hydrogen (H), molecular hydrogen ions (H_2^+), or neutral molecular hydrogen (H_2) [1,2] have been proposed to produce protonium.

Of vital interest to experimentalists planning measurement of the radiative decay spectrum of positronium is knowledge of the distribution of n and L values in which the system is produced. Calculating the collision processes leading to this formation is a three-, four-, or five-body problem for the cases of $\bar{p}$ on H, H_2^+, or H_2. Such few-body quantal calculations are challenging. Results have been presented for the three-body $\bar{p}pe$ system [3], but fully quantal calculations have not been reported for the four- and five-body systems.

Our semiclassical approach to collision modeling is motivated by the desire to better understand such many-body quantum-mechanical systems using the computationally tractable model originally developed by Wilets *et al.* to model nuclear matter [4,5] and later adapted to atomic problems by Kirschbaum and Wilets (KW) [6]; the KW approach has been applied to a variety of nuclear [7,8] and atomic [9–14] problems. The KW semiclassical model starts with a classical Hamiltonian, and then incorporates position- and momentum-dependent pseudopotentials to exclude particles from quantum-mechanically forbidden regions of phase space. In general, a "Heisenberg" pseudopotential prevents electron collapse into the nucleus while a "Pauli" pseudopotential holds electrons of like spin apart in phase space; for the present case of molecular hydrogen, we use only a two-center Heisenberg pseudopotential to prevent electron collapse into the protons.

As detailed in our previous work on atomic problems [9], proper design of the pseudopotential is fundamental to achieving an accurate representation of the target system, one which will have well-behaved collision dynamics. Before its use to study antiproton collisions, the molecular model is calibrated by adjusting pseudopotential parameters to reproduce experimental proton stopping powers at fixed collision energies.

Antiproton collisions are initially studied at fixed collision energies to verify model behavior, and to better understand the important features of $\bar{p}$-H_2 dynamics. We then examine the process of protonium formation in a cascade of collisions, in which the final energy of one collision is used as the next initial energy, much as we would expect in collision experiments, until the cascade ends with eventual antiproton capture, allowing analysis of protonium states from a realistic distribution of collision energies and impact parameters.

Collisions are performed over Monte Carlo initial conditions, which include separate solid body rotations and inversions of target positions and momenta, as well as randomization of the impact parameter b in equal areas of πdb^2 up to an empirically selected b_{max}. Our aim is to avoid affecting our results by restricting the range of initial conditions; thus we continue to expand the collision cascade, i.e., increase the value of the initial collision energy, the size of b_{max}, and the initial distance to the target at the start of each collision, until we see minimal changes in the overall capture process and products. Randomizing all collisions in a lengthy cascade

*Electronic address: beckb@microconnex.com

over the full cross-sectional area of impact parameters can involve significant amounts of computational time, but it allows a more confident analysis of collision products, from a realistically weighted distribution of initial conditions, than is achieved from a more limited selection of initial conditions.

Portions of this problem have been previously addressed by Cohen [13], who focused on an extension of the KW method to the H_2 molecule, positing multiple additional *ad hoc* pseudopotential terms to ameliorate what he found to be gravely overbound molecular ground states. By returning to the fundamentals of the KW method, in particular to the behavior of the Heisenberg pseudopotential in a multicenter molecule, we show that these additional terms are unnecessary to achieve a correctly bound ground state which can be used for accurate collision modeling. While our overall cross sections for protonium formation are similar to those calculated by Cohen over a fair range of collision energies, our mixes of collision products and of final protonium states are distinctly different, which we address in terms of the fundamentals of semiclassical collision modeling.

II. SEMICLASSICAL MODEL OF H_2

Our model of H_2 begins with the classical Hamiltonian, in the case of H_2,

$$H_{CL} = T + V_C = \sum_{i=1}^{2} \frac{p_i^2}{2} + \sum_{j=a}^{b} \frac{P_j^2}{2M} + \frac{1}{r_{12}} + \frac{1}{R_{ab}} - \sum_{i,j} \frac{1}{r_{ij}}, \quad (1)$$

where $\boldsymbol{r}_i, \boldsymbol{p}_i$, $i=1,2$, and $\boldsymbol{R}_j, \boldsymbol{P}_j$, $j=a,b$, are the electron and proton coordinates, with $r_{ij}=|\boldsymbol{r}_i-\boldsymbol{R}_j|$ and $p_{ij}\simeq|\boldsymbol{p}_i-\boldsymbol{P}_j/M|$; M is the proton mass and V_C is the net system Coulomb energy. We use atomic units with $e=m_e=\hbar=1$ throughout. This model is simple but unstable, as one electron will boil off while the other collapses into a proton. Adding our model of quantum-mechanical effects, a pseudopotential of the form

$$V_H(r,p) = \frac{\xi^2}{4\alpha r^2} \exp\{\alpha[1-(rp/\xi)^4]\}, \quad (2)$$

structures and stabilizes the semiclassical ground state by repelling the electrons from forbidden regions of phase space, in this case a core around each proton of size $\xi\hbar(\hbar=1)$ and hardness α:

$$H_{SC} = T + V_C + \sum_{i,j} \frac{\xi^2}{4\alpha r_{ij}^2} \exp\{\alpha[1-(r_{ij}p_{ij}/\xi)^4]\}. \quad (3)$$

This Hamiltonian minimizes to a symmetrical planar ground state, e.g., Fig. 1, in which the two electrons lie on the line bisecting the proton axis with $r_{12}=R_{ab}=1.574$, and have zero velocity but nonzero momentum,

$$\dot{\boldsymbol{r}}_i = 0 = \partial H/\partial \boldsymbol{p}_i = \boldsymbol{p}_i + \partial V_H/\partial \boldsymbol{p}_i; \quad (4)$$

$\dot{\boldsymbol{R}}_j$ and $\dot{\boldsymbol{P}}_j$ are also zero.

This ground state obeys a virial theorem, with the identification of $T+V_H$ as the effective kinetic energy T_{eff}:

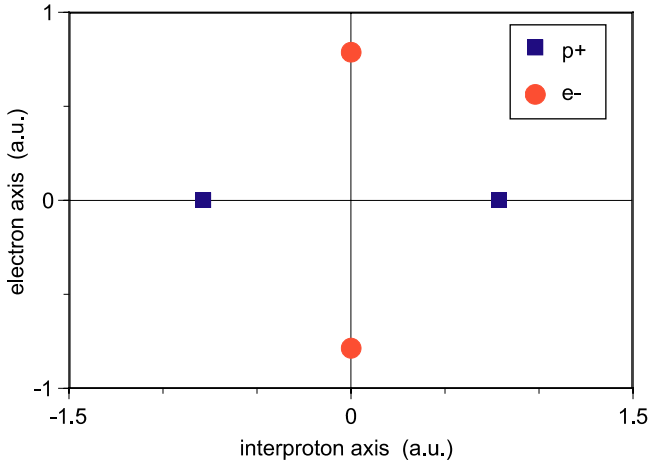

FIG. 1. (Color online) Symmetrical ground state for KW model of molecular hydrogen, $\alpha=1$, $\xi\simeq0.894$, $r_{12}=R_{ab}=1.574$.

$$E_{total} = E_{SC} = T + V_H + V_C = T_{eff} + V_C = V_C/2 = -T_{eff}. \quad (5)$$

As shown in Fig. 2, increasing core size ξ for fixed core hardness α expands the ground state, i.e., the r_{ij} $(=r_{12}/\sqrt{2}=R_{ab}/\sqrt{2})$ increase as the electrons are excluded from a larger core around each proton, and total system Coulomb attraction V_C, effective kinetic energy T_{eff}, and ground-state energy decrease, reaching the experimental ground-state energy of -1.174 a.u. for $\alpha=1$ and $\xi\simeq0.894$, the configuration of Fig. 1.

Note that this system minimizes to the correct ground-state energy without the several additional pseudopotential terms advocated by Cohen to avoid overbinding, by what he reported was a factor of 4 [13]. We find a continuum of choices available for pairs of the variables ξ and α which will minimize to the correct ground-state energy, as shown in Fig. 3, which plots a range of ground states with the correct total energy against the pseudopotential core hardness α. Se-

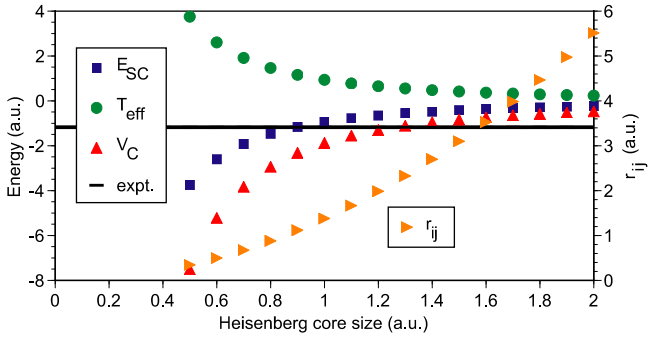

FIG. 2. (Color online) Minimized semiclassical system energies E_{SC} $(=T_{eff}+V_C)$, and corresponding ground-state electron-proton distances r_{ij}, plotted as a function of core size ξ for fixed core hardness $\alpha=1$. As core size increases, electrons are repelled further from the protons, and interaction energies decrease, matching the experimental H_2 ground-state energy for $\xi\simeq0.894$; all of these minimized model states obey the virial theorem $|E_{SC}|=T_{eff}$ $=-V_C/2$.

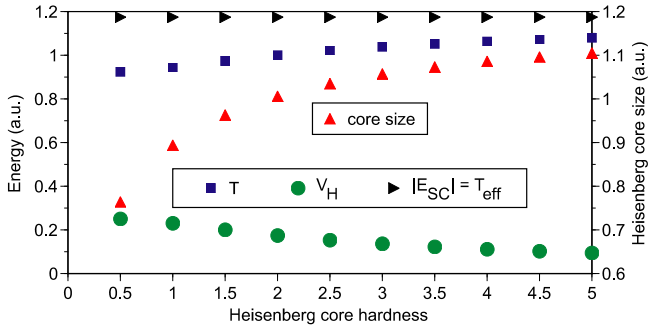

FIG. 3. (Color online) Range of ground states with the correct ground-state energy, plotted as a function of core hardness α. As core hardness increases and core interactions decrease, electron ground-state momentum and kinetic energy also increase as the core size ξ is increased to maintain the correct ground state size and energy.

lection among these ground-state candidates is made on the basis of collision dynamics, as will be discussed below.

Somewhat paradoxically, as Heisenberg core hardness is increased, there is less interaction between the electrons and the repulsive pseudopotential core, and binding energy increases. As a result, core size ξ must also be increased, thus increasing core repulsion, to maintain the same system configuration, Coulomb energy V_C and total system binding energy. Even so, as the core pseudopotential term V_H decreases with increasing core hardness, the electrons' ground state momentum and kinetic energy increase, maintaining the same effective kinetic energy $T_{eff}=|E_{SC}|=-V_C/2$.

Molecular binding energy curves are shown in Fig. 4. The H_2 ground-state binding energy is correct, with the potential well for interatomic separation somewhat broader than the Rydberg experimental values, as reported by Hirschfelder [15]. The model H_2^+ binding energy $\simeq$0.79 a.u., i.e., overbound relative to the experimental value, $\simeq$0.6 a.u., by somewhat less than 0.2 a.u., again more well behaved than the factor of 6 reported by Cohen. While one could tweak KW model parameters to replicate particular features of the ground state, e.g., the shape of the potential well, this is not our goal for this model, but rather to validate its use as a target for collision calculations. One could also adjust the

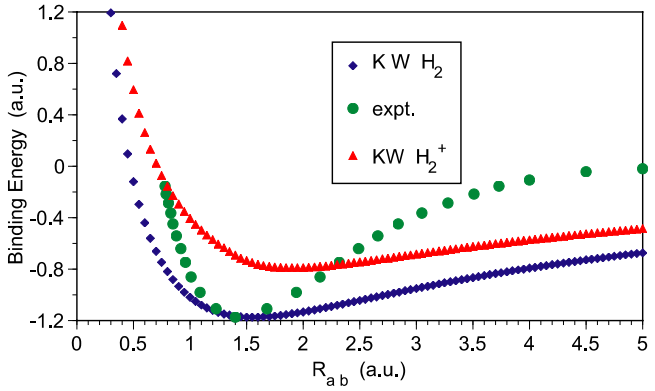

FIG. 4. (Color online) Molecular binding energy vs interatomic separation R_{ab}. The KW model shows a broader potential well than the experimental values, with H_2^+ overbound by $\lesssim$0.2 a.u.

model to include the $\frac{1}{2}\hbar\omega$ vibrational energy in the ground state, with ω determined from a quadratic fit to the potential well, and the correct vibrational momentum imparted to the protons; however, we found this correction to have negligible effect on collision results.

III. COLLISION CALCULATIONS AND STOPPING POWER

Minimizing to the correct ground-state energy leaves one free parameter in the model, which can be adjusted to modify the characteristics of the ground state. As is true for all simulations, our model's credibility hinges on the degree to which it can replicate experimental data. To validate our model for use in antiproton collision calculations, we first calibrate it against the well-documented proton stopping powers [16]. Proton collisions are performed by adding a proton (index c) to the semiclassical Hamiltonian,

$$H_{SC+P} = H_{SC} + P_c^2/2M - \sum_i \frac{1}{r_{ic}} + \sum_j \frac{1}{R_{jc}}, \tag{6}$$

and evolving the positions and momenta by integrating Hamilton's equations of motion, $\dot{\boldsymbol{r}}_i = \partial H/\partial \boldsymbol{p}_i$ and $\dot{\boldsymbol{p}}_i = -\partial H/\partial \boldsymbol{r}_i$, through the course of a collision.

A set of collisions is performed with Monte Carlo initial conditions to include separate solid-body rotations and inversions of both positions and momenta, and randomization of impact parameters with equal areas πdb^2 over the full range. From this ensemble, stopping power, defined as the integral over the impact parameter b of the energy loss times $2\pi b$, is calculated for a fixed initial energy E_0 as

$$\sigma\Delta E(E_0) = \pi b_{max}^2 \frac{1}{N}\sum_{i=1}^{N} \Delta E_i(E_0) \tag{7}$$

where $\Delta E_i(E_0)$ is the energy loss of the ith collision; statistical errors are

$$\delta(\sigma\Delta E) = \frac{\pi b_{max}^2}{\sqrt{N}}\left[\frac{\sum (\Delta E_i)^2}{N} - \left(\frac{\sum \Delta E_i}{N}\right)^2\right]^{1/2}. \tag{8}$$

Multiple collision sets are calculated, varying the maximum impact parameter b_{max} to verify that it does not affect the final results by limiting collision calculations to an inner region; we have again found this to be one of the essential factors in reproducing experimental stopping power data.

As demonstrated previously [9], the critical parameter for reproducing experimental stopping power is the core hardness α. As shown in Fig. 5, with twice as many pseudopotentials acting upon each electron in H_2, we find the best fit to experimental stopping powers with $\alpha=1$, i.e., half as strong as the $\alpha=2$ pseudopotentials used in our single-center atomic models. Stronger pseudopotentials, i.e., higher α, distort the stopping powers by more stiffly localizing the ground-state electrons, and increasing their ground-state momenta (see Fig. 3), resulting in unrealistically strong interactions and too large a momentum exchange with colliding protons. We thus fix our core hardness at $\alpha=1$ and adjust

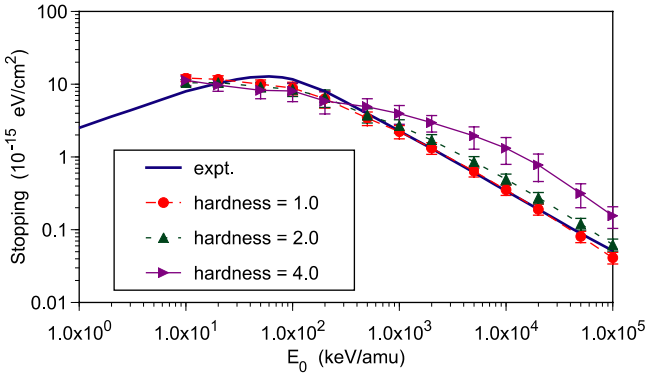

FIG. 5. (Color online) Proton stopping powers for different choices of core hardness α. Stopping powers increase with α, as electrons are fixed more rigidly, have greater ground-state momenta, and interact more strongly with the colliding protons; the two-center H_2 model fits experimental data with pseudopotentials half as strong as used in the atomic model.

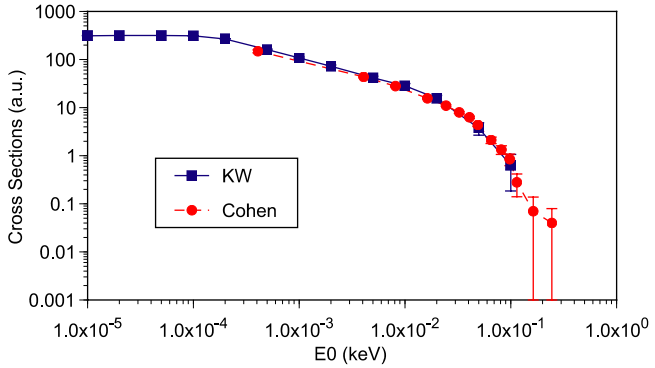

FIG. 6. (Color online) Total low-energy cross sections for protonium formation in the KW model, run with a maximum impact parameter of 10 a.u. In the range of 1–100 eV Cohen's results are quite similar to the KW model; at lower collision energies this KW simulation saturates, with all antiprotons captured into protonium for this b_{max}.

core size to $\xi \simeq 0.894$, which yields a ground state with the correct energy, stopping power and, as we would expect for a system with the correct ground-state energy, a good approximation to ground-state size, the symmetrical configuration shown in Fig. 1.

IV. ANTIPROTON CAPTURE AND THE COLLISION CASCADE

The Hamiltonian for antiproton collisions is the same as Eq. (6) with a sign change upon replacement of the proton projectile with an antiproton (index d),

$$H_{SC+\bar{P}} = H_{SC} + P_d^2/2M + \sum_i \frac{1}{r_{id}} - \sum_j \frac{1}{R_{jd}}. \tag{9}$$

Higher-energy stopping powers are similar to those calculated for protons, but with very limited product formation; above a collision energy of 100 eV ($\simeq$3.8 a.u.), we see statistically insignificant protonium formation. Our total cross sections for protonium formation at lower collision energies are shown in Fig. 6, calculated from 1000 collisions at each energy, distributed over a range of impact parameters up to $b_{max}=10$ a.u. (verification at $b_{max}=20$ a.u. showed similar results, although with larger statistical errors.) From a range of 1–100 eV our cross sections match well with those reported by Cohen; below ~0.2 eV our cross sections begin to saturate, with all antiprotons captured into protonium for these collision conditions.

Study of $\bar{p}-H_2$ interactions at fixed collision energies provides the opportunity to further develop the semiclassical model, and validate the discrimination and analysis of collision products (of which there can be a wide variety in the intermediate stages of a collision); however, the central question of what kinds of protonium states are likely to be actually formed remains open. In order to observe antiproton capture from a realistic distribution of collision energies and impact parameters, we employ a cascade of collisions, a method originally used in our earlier study of the formation of antiprotonic He. Starting with an initial energy well above the range in which antiproton capture can occur, we follow a sequence of collisions, using the final energy of one as the starting point of the next, with full Monte Carlo of the target configuration and impact parameter, until capture occurs. The initial conditions, most importantly the initial collision energy and the range of impact parameters, are again chosen so that they have negligible effects on the final distribution of collision products, but only on the number of collisions required to slow the antiprotons into the energy range from which capture occurs.

With a b_{max} of 10 a.u., we found during validation that the population of collision products stabilized for initial antiproton energies between 5 and 10 a.u., and thus began our collision cascade at an energy of 10 a.u. $\simeq$ 272 eV. Following this cascade long enough (average $\simeq$169 collisions from the start of a cascade until capture), we see two results:

(1) ~20% $\bar{p}+H_2 \rightarrow \bar{p}p+p+2e$, from higher E, lower b, and

(2) ~80% $\bar{p}+H_2 \rightarrow \bar{p}p+H+e$ from lower E, higher b.

Antiprotons at the end of the cascade, i.e., at the start of the collisions which will result in antiproton capture, have collision energies ranging from 0.004 to 9.9 a.u. (0.11–269 eV), with the bulk of the population below 2 a.u. (median value of 1.08 a.u. $\simeq$ 29.4 eV), as shown in Fig. 7.

Figure 8 plots the energy and angular momentum distribution of these antiprotons, about to be captured into the protonium states shown in Fig. 9, which plots the distribution of protonium quantum number n against angular momentum (and quantum number) L, (1) $n=\sqrt{M^*/2|E|}=\frac{1}{2}\sqrt{M/|E|}$, $\langle n\rangle \sim 29.5$, $\delta_n \sim 13$; (2) $\boldsymbol{L}_{jd}=\boldsymbol{R}_{jd}\times\boldsymbol{P}_{jd}$, $\langle L/n\rangle \sim 0.68$, $\delta_{L/n} \sim 0.24$, where $M^*=M/2$ is the effective mass of the protonium molecule. It can be seen that the higher-energy, lower-impact-parameter collisions are more likely to result in double ionization of the target H_2 molecule. Note that these collisions result in a similar distribution of protonium states ($\langle n\rangle \sim 29.1$, median $n \sim 23.2$, $\langle L\rangle \sim 18.1$) to the majority of protonium atoms formed from the generally lower-energy, higher-impact-parameter collisions leading to antiproton ex-

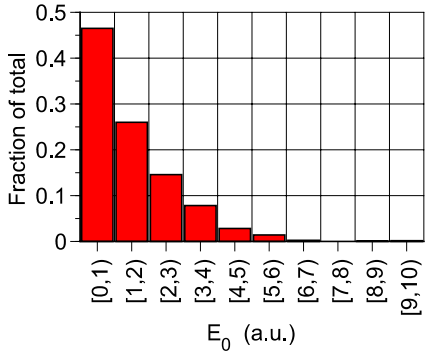

FIG. 7. (Color online) Histogram of antiproton energies at the end of the collision cascade; antiprotons with energies below about 2 a.u. are most likely to be captured.

change with a single electron, leaving a free H atom ($\langle n \rangle \sim 29.8$, median $n \sim 26.7$, and $\langle L \rangle \sim 20.2$); note also that these protonium atoms stack up against the $L=n$ centrifugal barrier, as expected for a semiclassical treatment.

The broad and smooth distribution of capture states results from the broad range of collision conditions leading to antiproton capture at the end of the collision cascade. This distribution is also seen in the histogram of Fig. 10. This is in contrast to the treatment of Cohen [13], which showed a significantly narrower distribution, δ_n of 3–4, peaked around $n \sim 25$.

As can be seen from Fig. 8, most antiproton captures occur from fairly low energies and/or impact parameters, resulting in decreasing protonium formation for collision energies much above a couple of atomic units, consistent with the fixed energy results shown in Fig. 6.

V. COMPARISON WITH THE COHEN APPROACH

This work was motivated by questions posed to us by members of the experimental community, regarding the earlier analysis of this problem by Cohen [13]. As the originators and developers of the KW model, we were concerned that Cohen had found it to be unsuitable for this molecular application, despite our own earlier work with a KW model of H_2O [9].

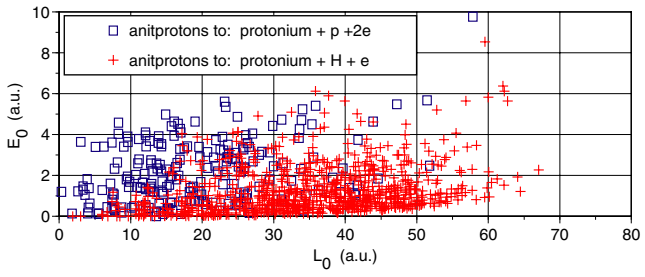

FIG. 8. (Color online) Distribution of antiproton E and L at the start of the collisions resulting in antiproton capture; the higher-energy, lower-angular-momentum (smaller-impact-parameter) antiprotons are more likely to result in protonium formation via complete ionization of the H_2 molecule.

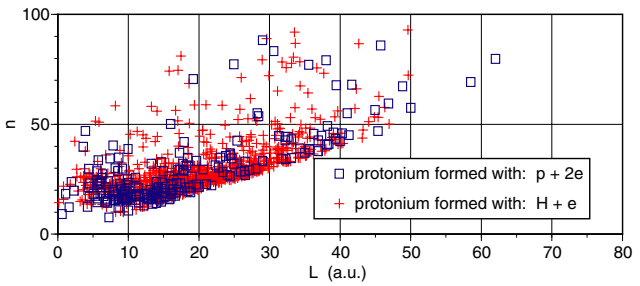

FIG. 9. (Color online) Protonium n and L states resulting from the antiproton distribution of Fig. 8. Protonium atoms formed by single and double ionization of H_2 show similar overall distributions of final states, with somewhat more scatter in those formed via double ionization.

A. Basic features of the model

Cohen begins with an assertion that the KW model overbinds molecular hydrogen by a factor of 4 (or 6 for H_2^+) because it produces a symmetrical ground state with unrealistically tight electron and proton separations of $r_{12}=R_{ab} \simeq 1.2$ a.u., and proceeds to correct the model's misbehavior by adding multiple additional pseudopotentials to repel the electrons from multiple additional positions in the molecule. We find these modifications unnecessary, and not in accord with the Heisenberg and Pauli principles on which the KW model is based; the role of the pseudopotential of Eq. (2) is to exclude electrons from quantum mechanically forbidden regions of phase space.

As discussed above in Sec. II, and illustrated in Figs. 2 and 3, the KW model readily assumes the proper ground-state size, with proton spacing of $R_{ab} \simeq 1.57$ a.u., and thus the desired binding energy, with an appropriate choice of the core size ξ and hardness α. Indeed, determining the range of model parameters which result in the correct ground-state energy is the first step in designing any such semiclassical model. There is a continuum of choices which achieve the correct static ground-state binding energy, and, by the virial theorem, none which achieve it without the proper size, since the ground-state energy is just one-half the total Coulomb energy of the system, $E_{SC}=V_C/2$, and is thus a function of the particle separations, as seen in Eq. (1). While additional model parameters provide additional degrees of freedom to

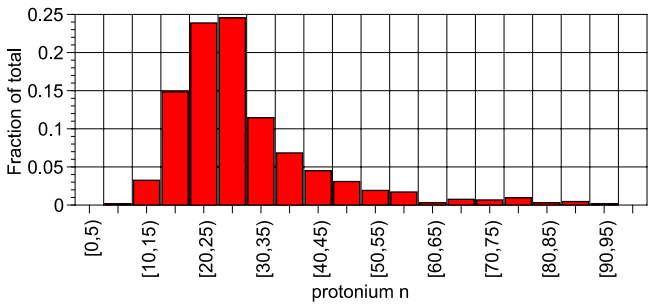

FIG. 10. (Color online) Histogram of protonium n; the broad distribution in n results from the broad range of range of energies and impact parameters at the end of the collision cascade which result in capture.

fit molecular potentials, for use as a target in collision studies we find no undesirable features of the symmetrical ground state produced by the KW model.

Examining the collision dynamics of the KW model, we find, as in our previous work [9,10], that it is the core hardness α which determines the model's ability to reproduce experimental stopping power. In a properly distributed set of model initial conditions, the interesting events occur in the small fraction of collisions which align in phase space to result in significant momentum exchange between the projectile and elements of the target system, as is observed experimentally. When the semiclassical ground-state is overconstrained by use of an excessively strong core hardness α, which increases ground-state electron momentum, these well-aligned collisions result in unrealistically high momentum transfer, and a greater number of more interesting events than would occur naturally. This is easily seen from the effect of core hardness on stopping power in Fig. 5, but is also observed in other metrics, such as the cross sections for H_2 ionization and splitting, and, centrally, on the rate of protonium formation, which in our own treatment increased by a factor of approximately 200 following an increase of core hardness α from 1 to 4, for 1000 collisions run at an initial laboratory energy of 100 eV $\simeq$ 3.7 a.u.

B. Initial collision conditions

Cohen reports that his collisions commence with the projectile at a distance of 10 a.u. from the target center. In validation of our own model, we found differences in collision dynamics and overall results with collisions starting this close to the target, where the effect of instantaneously depositing a projectile, and the resulting step function in Coulomb interactions, is non-negligible. We found these differences to wash out at starting distances of 50–100 a.u., and thus started all collisions at 100 a.u.; while computationally more time consuming, our guiding principal was to expand our initial collision conditions until they had minimal effect on the overall results.

This principal also guided our use of a continuous distribution of impact parameters in db^2, up to a b_{max} chosen not to affect overall results. It is possible to achieve correct results by segmenting impact parameter space into a set of rings around the target center, however we found that this approach tended to produce an overall early convergence resulting from the appealing efficiency of undersampling the outer rings, which then diverged upon more fully exploring the overall impact parameter space. We are reassured that the results in this case are surprisingly close to those of the KW model in the middle energy range, but would be interested in cross sections for the Cohen model calculated for continuous distributions over wider ranges of impact parameter space.

C. The collision cascade

Beyond these issues, however, is the central question of the overall distribution of collision conditions used to study protonium formation. We find a cascade of collisions to be the most reasonable method of selecting a realistic ensemble of preformation states, and attribute the narrow distribution of protonium states reported by Cohen, along with the limited observation of the complete dissociation reaction $\bar{p}+H_2 \rightarrow \bar{p}p+p+2e$, to the use of discrete initial energies, compounded by limited sampling of impact parameters. Limiting the range of energy and angular momentum states going into the collision process will inevitably restrict the range of products formed, while starting with fixed initial energies will result in a peaked distribution of n states; observation of these effects in our own early work has guided development of our present approach to collision modeling, which we find more effective at reducing model effects on overall results.

VI. SUMMARY AND FUTURE PROSPECTS

By returning to the fundamentals of semiclassical modeling, i.e., working out the detailed behavior of the pseudopotentials used to stabilize an additional application, and then calibrating the model against experimental collision data, we have extended the single-centered treatment of atomic targets to molecular hydrogen without the *ad hoc* introduction of additional terms which unnecessarily complicate the model, and which have the potential to distort collision results in an as yet unexplored fashion.

Calibrating a model against experimental data is the crucial step in any simulation, and is what allows us to examine protonium formation in the antiproton-H_2 collision system with increased confidence that our model is not unduly distorting results. The low-energy cross sections for protonium formation and the wide distribution of protonium states inform the experimentalist where and how hard it may be necessary to search for these collision products. Future work on this problem will include more detailed examination of collision products and their postcollision trajectories, to further aid in design of collision experiments.

ACKNOWLEDGMENTS

This work was motivated by discussions at LEAP03, and aided by discussions at LEAP05; we would like to acknowledge the opportunities provided by the organizers of these meetings, including financial support to attend LEAP05, and the contributions to our understanding of antiproton physics resulting from discussions with the participants of these meetings.

[1] J. Eades and E. Hartman, Rev. Mod. Phys. **71**, 373 (1999).
[2] M. Holzscheiter and M. Charlton, Rep. Prog. Phys. **62**, 1 (1999).
[3] X. Tong, T. Watanabe, D. Kato, and S. Ohyani, Phys. Rev. A **64**, 022711 (2001).
[4] L. Wilets, E. M. Henley, M. Kraft, and A. D. Mackellar, Nucl. Phys. A **282**, 341 (1977).
[5] L. Wilets, Y. Yariv, and R. Chestnut, Nucl. Phys. A **301**, 359 (1978).
[6] C. L. Kirschbaum and L. Wilets, Phys. Rev. A **21**, 834 (1980).
[7] D. Callaway, L. Wilets, and Y. Yariv, Nucl. Phys. A **327**, 250 (1979).
[8] J. Kunz, R. Babinet, L. Wilets, and U. Mosel, Nucl. Phys. A **367**, 459 (1981).
[9] W. A. Beck and L. Wilets, Phys. Rev. A **55**, 2821 (1997).
[10] W. A. Beck, L. Wilets, and M. A. Alberg, Phys. Rev. A **48**, 2779 (1993).
[11] J. S. Cohen, Phys. Rev. A **51**, 266 (1995).
[12] J. S. Cohen, Phys. Rev. A **54**, 573 (1996).
[13] J. S. Cohen, Phys. Rev. A **56**, 3583 (1997).
[14] L. Wilets and J. Cohen, Contemp. Phys. **39**, 163 (1999).
[15] J. Hirschfelder, C. Curtiss, and R. Byrd, *Molecular Theory of Gases and Liquids* (Wiley, New York, 1954).
[16] H. H. Andersen and J. F. Ziegler, *Hydrogen Stopping Powers and Ranges in All Elements* (Pergamon Press, New York, 1977).